Meteorol. Z. (Contrib. Atm. Sci.), Vol. **33**, No. 2, 145–157 (published online February 29, 2024)

Calculation of aerosol particle hygroscopic properties from OPC derived PM2.5 data

Vasileios Savvakis*, Martin Schön, Matteo Bramati, Jens Bange and Andreas Platis

Eberhard Karls Universität Tübingen, Germany

(Manuscript received March 20, 2023; in revised form December 26, 2023; accepted January 1, 2024)

Abstract

Hygroscopic growth of aerosol particles due to increasing relative humidity in the atmosphere is characterized by their hygroscopicity parameter κ and their hygroscopic growth factor GF. A technique to calculate the two using $PM_{2.5}$ data from two optical counting sensors is examined. Only one of the two instruments is equipped with a drying channel, and therefore differences between ambient and dry air concentrations can be observed when both are working simultaneously. Based on the definition of the hygroscopic growth factor as the ratio between an aerosol particle's wet and dry diameter, a relationship including PM values is reached through the assumption of particle spherical shape and basic geometry. Aerosol particles from marine and urban sources were sampled during a week of measurements in two locations, in Norderney, Germany during April 2021 and in Rødby, Denmark, during September 2022. Calculated GF and κ values were related to the origin of the air mass using back trajectory modeling (NOAA HYSPLIT) and by comparing the results to their expected values and fits on theoretical growth curves. It was found that $\kappa = 0.6 \pm 0.1$ when continental air was sampled (agreeing with ammonium sulphate's $\kappa = 0.61$) and $\kappa = 1.1 \pm 0.1$ when marine air was sampled (agreeing with sea salt's same value). The GF estimates also matched their respective expected values within a deviation of 1σ. For the measurements in Rødby, particle number size distributions for the cases of marine sourced concentrations showed a peak at 1 to 2 µm, which is similar to previous studies of Baltic sea aerosol particle size distribution and structure.

Keywords: hygroscopic growth, hygroscopicity parameter, optical particle counter, marine aerosol, urban aerosol

1 Introduction

The vast majority of aerosol particles grow in apparent size due to water uptake from the environment in conditions of increasing moisture in the air (Svennings-son et al., 2006; Laskina et al., 2015; Davies et al., 2021). This phenomenon, often called hygroscopicity, is characteristic of aerosol particle chemical composition (Gysel et al., 2007; Tang et al., 2019). Among others, studies have been conducted related to the hygroscopic growth of diesel soot (Weingartner et al., 1997), mineral dust (Kaaden et al., 2009), ammonium sulphate (Hämeri et al., 2000), pollen (Griffiths et al., 2012), sea salt (Ming and Russell, 2001; Zieger et al., 2017) as well as pure sodium chloride (Hämeri et al., 2001; Biskos et al., 2006).

For aerosol particle concentrations monitoring, optical particle counters (OPCs) are widely used as they usually cover a sufficient size range for air quality assessment and can provide information on particulate matter (PM) types like PM_1, $PM_{2.5}$ and PM_{10}. While high end instrumentation of this type often features internal treatment of the hygroscopic growth effect by employment of drying methods, low-cost OPCs do not inherently deal with the issue. As a result, relative humidity (RH) related mathematical corrections have been developed for adjusting the data during post-processing (Di Antonio et al., 2018; Crilley et al., 2020; Malings et al., 2020). They rely on certain assumptions about the characteristics of the sampled air mass, which remains unknown. To give information on aerosol size, OPCs work on the principle of Mie scattering theory (Drake and Gordon, 1985; Bohren and Huffman, 2008), and aerosol identification is not directly possible. Deeper insight on aerosol particle type could be achieved, if instruments with and without a drying component operate at the same time and analysis is performed based on their output difference, which comes from evident hygroscopicity at humid conditions.

In the sub-micrometer range, aerosol particle humidification has been studied most commonly by using a Hygroscopic Tandem Differential Mobility Analyzer (H-TDMA) (Swietlicki et al., 2008; Kitamori et al., 2009), which was developed following the influential work of Liu et al. (1978), who first introduced the concept. For larger size ranges, other methods that have been attempted include directly collecting particles with a cascade impactor, e.g. Hitzenberger et al. (1997); Turšič et al. (2006), or combining in-situ RH and aerosol data from an aircraft, and a vertical scan-

*Corresponding author: Vasileios Savvakis, Eberhard Karls Universität Tübingen, Department of Geosciences, Schnarrenbergstraße 96, 72076 Tübingen, Germany, e-mail: vasileios.savvakis@uni-tuebingen.de

ning LIDAR for estimation of the scattering enhancement factor f for up to sizes of 3 µm (Feingold and Morley, 2003). Hegg et al. (2006) first presented a hygroscopicity study using airborne OPC data, which extended up to 3.5 µm, by comparing particle size distributions from a highly humid air sample (around 90 % RH) and one at a drier state (around 50 %), both collected with the two OPCs on board an aircraft on the east coast of California, United States. In their work, both marine and polluted aerosol sources were examined and it was verified that marine aerosols are generally more hygroscopic than ones found in urban centers. A similar approach of aircraft based OPC measurements, one featuring a drying chamber and one operating without it, was conducted by Snider and Petters (2008), who investigated aerosol spectral densities and derived growth factor (GF) values from the dried / non-dried data, by addressing possible sources of uncertainty like particle shape, refractive index and aerosols being chemical solutions of different components. Additional studies using direct PM data for inspecting hygroscopicity have focused on the changes in scattering enhancement due to increased moisture and have been related to visibility (Zhao et al., 2019; Molnár et al., 2020; Won et al., 2021).

The objective of this work is to investigate how accurately the hygroscopic GF can be calculated from direct PM readings, for example $PM_{2.5}$, based on a set of calculations starting from the formula definition of GF. Previous studies have followed different approaches after conceiving the concept, and used measurements from manned airborne platforms or direct aerosol particle collection. This method is still based on solely two sensors with the same measurement principle, and the use of their direct PM output. One of the two should feature a drying chamber, either self-constructed as a modification to a sensor that doesn't have one (Savvakis et al., 2024), or internally adjusted by the manufacturer as an extra component. Measurements of $PM_{2.5}$ can be collected from one sensor with a drying chamber at the same time with another sensor without a drying chamber, and based on the observed differences, a GF value can be calculated. Previous related studies have approached this problem by analysing aerosol particle size distributions and the differences between wet / dry case, however a PM value is generally more accessible and more foundational regarding particulate matter. As many low-cost sensors do not have a high number of size bins that is required for an accurate size distribution, such an analysis is often not possible. In this paper, we examine whether calculating hygroscopic properties of aerosol particles and unveiling details on the origin of the sampled air mass, is possible solely from PM data, a universally shared sensor output. The description of the parameters and derived formulas is described in Section 2.1, and then results from the measurements in two locations, in the North Sea (Norderney island), and the Baltic Sea (Rødby port), where the method and analysis was applied, are presented in Section 3.

2 Materials and methods

2.1 Theory

2.1.1 Hygroscopic growth

For an aerosol particle, GF is defined via the ratio between its wet diameter in ambient conditions and its dry diameter under conditions of low RH, below its efflorescence point:

$$\mathrm{GF} = \frac{d_w(\mathrm{RH})}{d_d} \tag{2.1}$$

According to Eq. (2.1), this ratio will be above unity when $d_w > d_d$, essentially when conditions are humid enough for the aerosol particle to adsorb water vapor from its surroundings. At dry conditions, $d_w = d_d$ and therefore, GF = 1. A formula has been developed for calculating GF only as a function of RH and by introducing a hygroscopicity parameter κ, first introduced and analysed by Petters and Kreidenweis (2007):

$$\mathrm{GF} = \left(1 + \kappa \cdot \frac{a_w}{1 - a_w}\right)^{\frac{1}{3}} \tag{2.2}$$

In Eq. (2.2), a_w is the so-called water activity, which is defined as the dimensionless ratio between the water vapor pressure of water in the solution and the vapor pressure of pure water, i.e. RH over the Kelvin effect. For deriving Eq. (2.2), the Kelvin effect has been omitted, as it is only important for aerosol particles of sizes in the nanometer range (Fitzgerald, 1975; Snider and Petters, 2008). Therefore, in this case a_w is reduced to:

$$a_w = \frac{\mathrm{RH}}{100} \tag{2.3}$$

In the past, potential values for the hygroscopicity parameter κ, at urban and marine environments, have been thoroughly examined. Marine air predominantly consists of sea salt with $\kappa = 1.1$ (Zieger et al., 2017; Hagan and Kroll, 2020). Urban air masses can be more mixed, and following the conceptual approach of Di Antonio et al. (2018), $\kappa = 0.61$ can be considered as a reasonable value for a typical polluted environment with the assumption that it consists mainly of ammonium sulphate. By considering an efflorescence point of RH = 35 % (or $a_w = 0.35$) for ammonium sulphate (Di Antonio et al., 2018) and RH = 45.6 % (or $a_w = 0.456$) for sea salt (Gupta et al., 2015), the GF relationship to increased RH for all possible cases can be calculated by using Eq. (2.2)–(2.3) and the aforementioned κ values. Figure 1 shows the result for the two different compounds. Since κ is higher for sea salt than for ammonium sulphate, its GF curve is also higher in Figure 1, i.e. a sea salt particle attracts more water vapor than an ammonium sulphate particle at the same RH conditions. Sea salt can have multiple salts and a consequently more complex hygroscopic nature that would

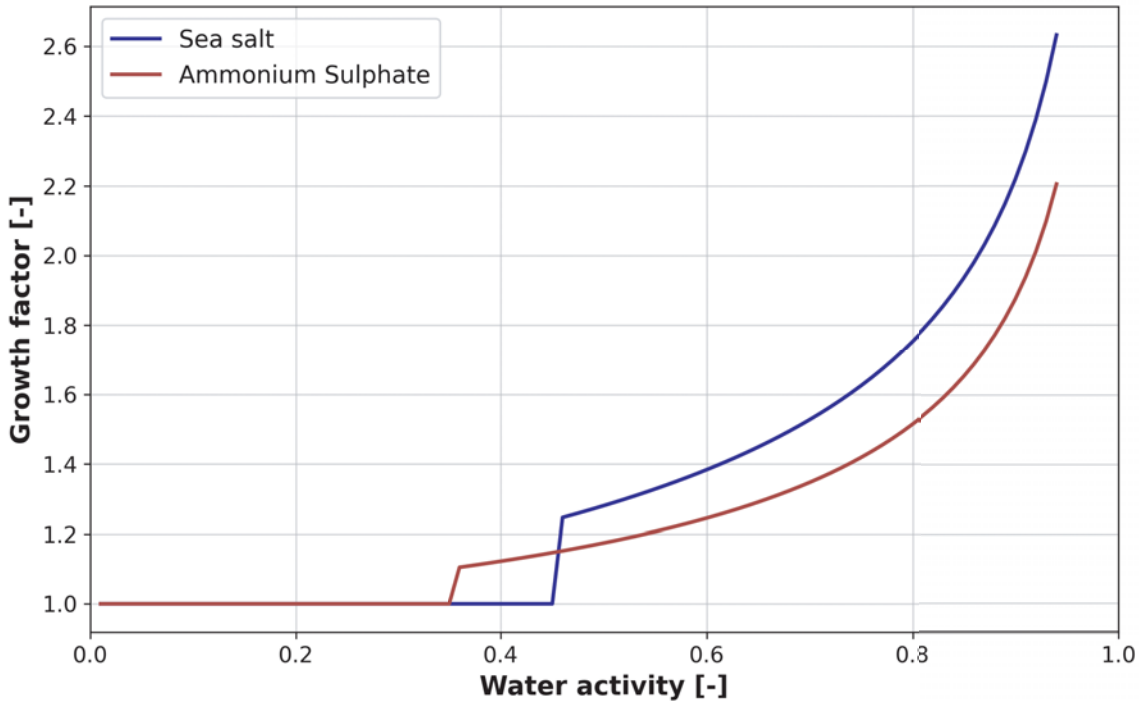

Figure 1: Growth factors for values of a_w between 0.2 and 0.95, produced by using Eq. (2.2) and by taking into account the two efflorescence points for ammonium sulphate (35 %) and sea salt (45.6 %). Below these boundaries, the RH conditions are low enough for the aerosol particle to not attract any water vapor, hence its growth factor is equal to unity.

not be described by a singular efflorescence point. This means that measured sea salt may still contain water content below the 45.6 % point depicted in Figure 1. Nevertheless, for the purposes of this study, the efflorescence point of sodium chloride was considered for the case of sea salt, as its preeminent component, and with similar hygroscopic behavior (Tang et al., 1997).

2.1.2 Calculation of GF from PM measurements

Based on Eq. (2.1), the following steps can be made to attain an expression with PM types starting from d_w and d_d, by assuming that the aerosol particles are spherical, and therefore of a known volume formula:

$$\begin{aligned} \mathrm{GF} = \frac{d_w}{d_d} &= \left(\frac{V_w}{V_d}\right)^{\frac{1}{3}} = \left(\frac{V_d + V_{\mathrm{water}}}{V_d}\right)^{\frac{1}{3}} \\ &= \left(1 + \frac{V_{\mathrm{water}}}{V_d}\right)^{\frac{1}{3}} = \left(1 + \frac{\frac{\mathrm{PM}_{\mathrm{water}}}{\rho_{\mathrm{water}}}}{\frac{\mathrm{PM}_d}{\rho_d}}\right)^{\frac{1}{3}} \\ \Rightarrow \mathrm{GF} &= \left(1 + \frac{\rho_d \cdot \mathrm{PM}_{\mathrm{water}}}{\rho_{\mathrm{water}} \cdot \mathrm{PM}_d}\right)^{\frac{1}{3}} \end{aligned} \tag{2.4}$$

In the final expression (Eq. (2.4)), ρ_{water} is the density of water, $\mathrm{PM}_{\mathrm{water}}$ is the mass of the water layer around the aerosol particle, PM_d its solid (i.e. real) size and ρ_d is the density of the dry particle. The calculation above assesses that the total PM value of a wet aerosol particle exists as a meta-stable solution between dry core and water uptake, meaning that the two layers neighbor but do not mix, hence the concept of adsorption (Sorjamaa and Laaksonen, 2007). As principles of physical chemistry can make clear statements about aerosol state and composition (that for example, sea salt is an aqueous well-mixed solution), this procedure represents an approximation. Based on that, $\mathrm{PM}_{\mathrm{water}}$ is estimated as:

$$\mathrm{PM}_{\mathrm{water}} = \mathrm{PM}_w - \mathrm{PM}_d \tag{2.5}$$

where PM_w is the ambient PM measurement and PM_d is the dry PM measurement. These two quantities, and in return $\mathrm{PM}_{\mathrm{water}}$ from Eq. (2.5), correspond to an OPC measurement without and with a drying chamber, respectively.

When calculating GF in this way, the dry particle density ρ_d is still required, which demands knowledge on the type of particles measured. However, theoretical densities of different elements are known in literature and can be tested through Eq. (2.4). Since the difference between PM_w and PM_d in a specific measurement time is dependent on the type of air being sampled, only the appropriate particle density value will match its corresponding GF curve from Figure 1. A verdict of the air mass type during the measurements can then be drawn by using only PM data from the two OPCs and the theoretical GF curve shown in Figure 1, which here displays two components representative of urban polluted (ammonium sulphate) and marine (sea salt) air content.

Table 1: Date, location, starting and ending time of data collection for all measurements. For each case, the air mass gets a classification as either "Marine" which corresponds to an origin from the sea, or "Urban" for an origin from land, according to the 24-hour back trajectories done with HYSPLIT and shown in Figure 2–3. "Dry" refers to PM data from an OPC with a drying chamber, i.e. PM_d, and "Ambient" to PM data from an OPC without a drying chamber, i.e. PM_w.

Date	Location	Ambient	Dry	Start UTC	End UTC	Air mass [HYSPLIT]
17 Apr 21	Norderney	OPC-N2	OPC-N2+dryer	07:09	08:12	Marine
16 Sep 22	Rødby-Land	OPC-N3	Fidas Fly 100	16:40	19:14	Marine
17 Sep 22	Rødby-Land	OPC-N3	Fidas Fly 100	07:17	09:16	Marine
21 Sep 22	Rødby-Vessel	OPC-N3	OPC-N3+dryer	11:38	12:34	Marine
19 Apr 21	Norderney	OPC-N2	OPC-N2+dryer	09:42	10:44	Urban
19 Sep 22	Rødby-Land	OPC-N3	Fidas Fly 100	17:15	19:12	Urban
22 Sep 22	Rødby-Vessel	OPC-N3	OPC-N3+dryer	12:27	13:15	Urban
23 Sep 22	Rødby-Land	OPC-N3	OPC-N3+dryer	10:30	11:15	Urban

2.2 Instrumentation

Two low-cost OPCs were employed, the OPC of type N2 (Alphasense, 2015) and N3 (Alphasense, 2019), which are both very similar in terms of dimensions and operation. The sensors feature their own micro-fan for active aspiration and cover a range of 0.38–17 µm with 16 size channels (OPC-N2) and 0.35–40 µm with 24 size channels (OPC-N3), and provide output of PM data based on raw size channel bins and their own internal algorithms. Both the OPC-N2 and OPC-N3 have an operational range of 0–95 % RH, according to the manufacturer. Furthermore, the optical aerosol spectrometer (OAS) Fidas Fly 100 (Palas, Karlsruhe, Germany) was also used, a high-end instrument with similar operational philosophy that covers a size range of 0.18 to 18 µm through 264 channels. Since the OPC-N2/N3 do not include a technique for drying the sampled air, they were used for measurements of ambient air, i.e. including moisture, while the Fidas Fly 100 was used for capturing dry PM concentrations, as it features its own internal dilution dryer, the Intelligent Aerosol Drying System (IADS).

Humidity was measured with the miniaturised T/RH sensor named SHT31 (Sensirion, Switzerland), which operated simultaneously along the OPCs. The SHT31 comes pre-calibrated and operates at the whole RH range, with a response time of 8 s and typical error of 2 % for humidity (Sensirion, 2016). Its measurement principle is based on capacitive humidity sensing, i.e. RH is determined from the capacitance change of a dielectric material between two electrodes, as a response to moisture absorption. At times, only the two low-cost OPCs operated for intercomparison, and in this case self-constructed diffusion drying channels were installed on one of the sensors only. Details on the setup of each measurement time period can be found in Table 1. Both instruments' function, along with the RH sensor, was supported by the use of a companion computer (Raspberry Pi 3b*), which handled the data acquisition and saving of the output files at a frequency of 1 Hz. The OPC-N2/N3 and the Fidas Fly include embedded algorithms for the calculation of PM types from raw bin counts, and only direct $PM_{2.5}$ readings were taken for the calculations of this study.

2.3 Measurement locations

The first measurement location was at the north side of Norderney island, Germany (coordinates: 53.7229, 7.2116) for two days in April (17th and 19th), 2021 and the second location was outside of the town of Rødby, Denmark and near Hyldtofte Østersøbad beach (coordinates: 54.6385, 11.4158), lasting one week in September, 2022. Both locations are in maritime environment (North and Baltic Sea), granting the chance of sampling marine based air, and the experimental periods were chosen to cover spring and autumn. During days of southerly winds, air masses from the land (e.g. Germany or Poland respectively) can arrive in both these spots, carrying continental sourced aerosol particles. The difference between maritime / urban air can be seen in their hygroscopic behavior. Similar but not identical rates of hygroscopic growth should become visible under humid conditions between these two cases, as the included elements have different values for κ, as seen in the two characteristic lines of Figure 1. Measurements were taken for time periods of 30 minutes to 2 hours throughout the span of the week in the morning or late evening of the day, for capturing the higher humidity conditions at night. Alongside the two main sensors, RH data was collected through an SHT31 (Sensirion, Switzerland) miniaturised meteorological sensor working in parallel, which operated at a sampling rate of 2 s, the same as the OPC-N2/N3 and Fidas Fly 100. The total of all measurement periods are summarised in Table 1. 24-hour back trajectories of the air mass at the time of measurements were acquired through the NOAA Hybrid Single-Particle Lagrangian Integrated Trajectory (HYSPLIT) model (Stein et al., 2015) at three different altitudes above sea level: 10, 200 and 500 m, to track the source of the measured aerosol particles, be it of marine or urban origin. The back trajectories can be seen in Figure 2a–3.

For each measurement day, $PM_{2.5}$ data were collected from the ambient air using an instrument without a drying chamber (third column in Table 1) and the

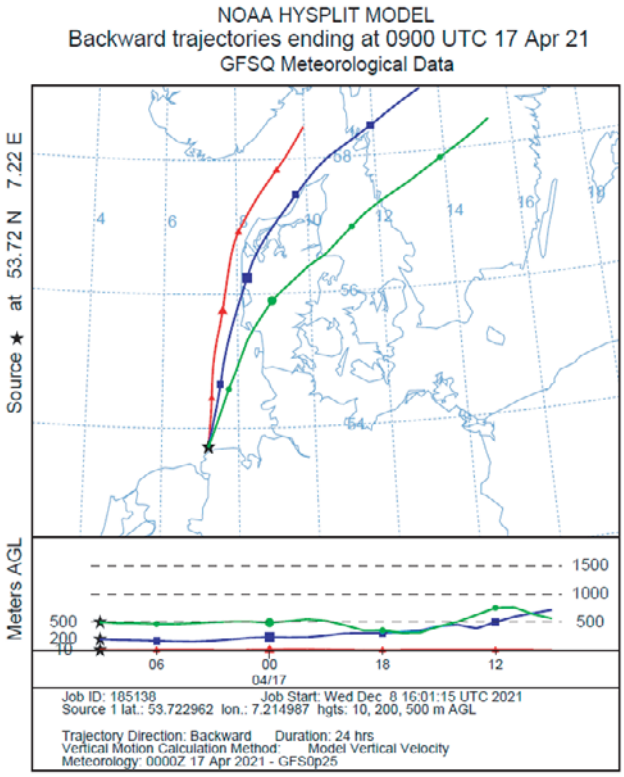

(a) 17th of April, 2021 (Norderney).

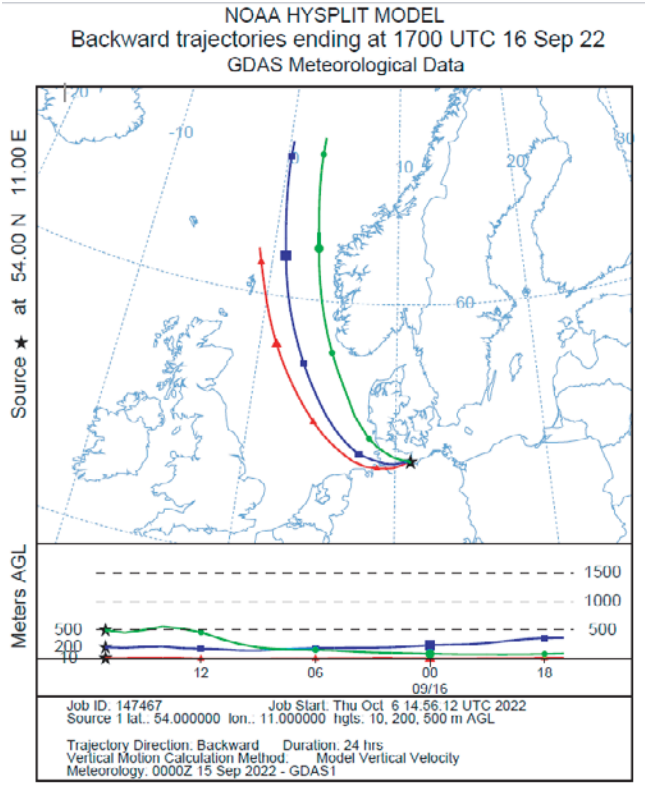

(b) 16th of September, 2022 (Rødby).

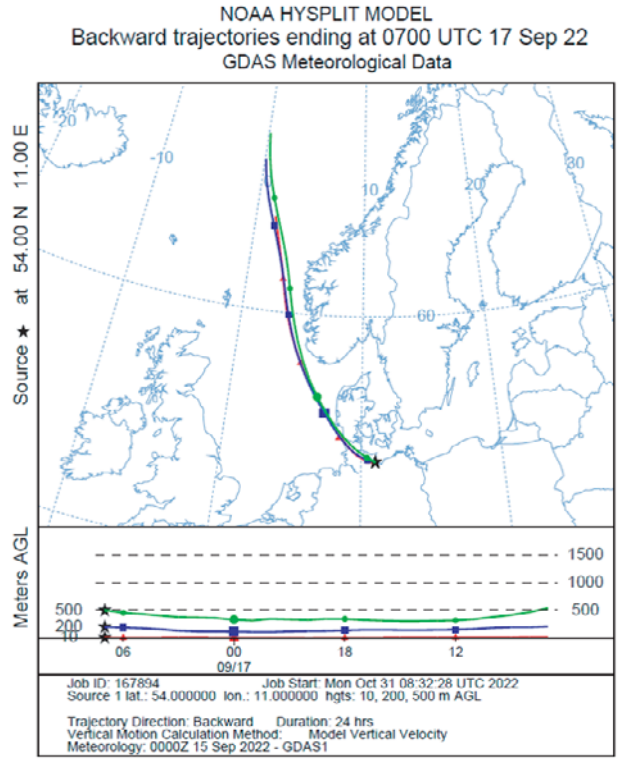

(c) 17th of September, 2022 (Rødby).

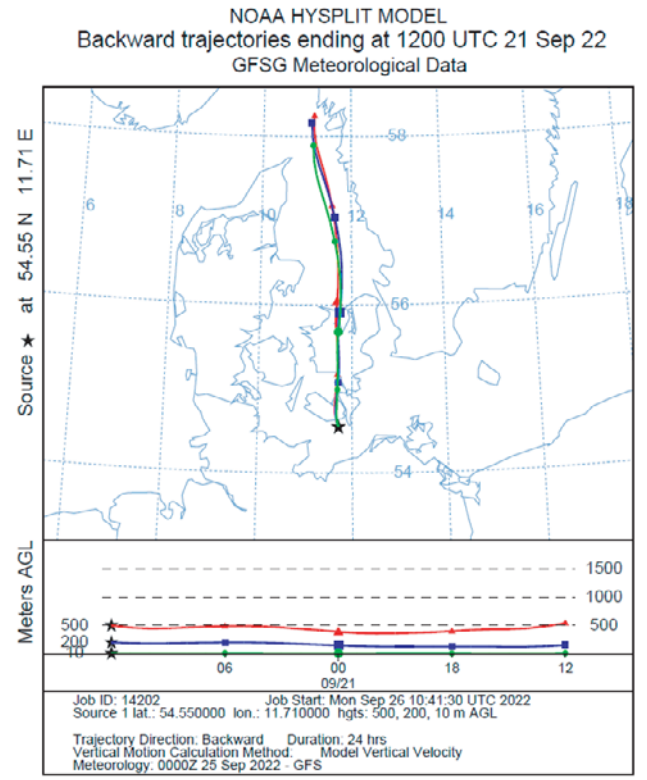

(d) 21st of September, 2022 (Rødby).

Figure 2: Air mass 24-hour back trajectories for the cases of a marine aerosol source. The black star denotes the measurement location, which is also captioned below each figure, and the three lines indicate the origin of the air mass at three different altitudes, 10 m (light green), 200 m (dark blue) and 500 m (red).

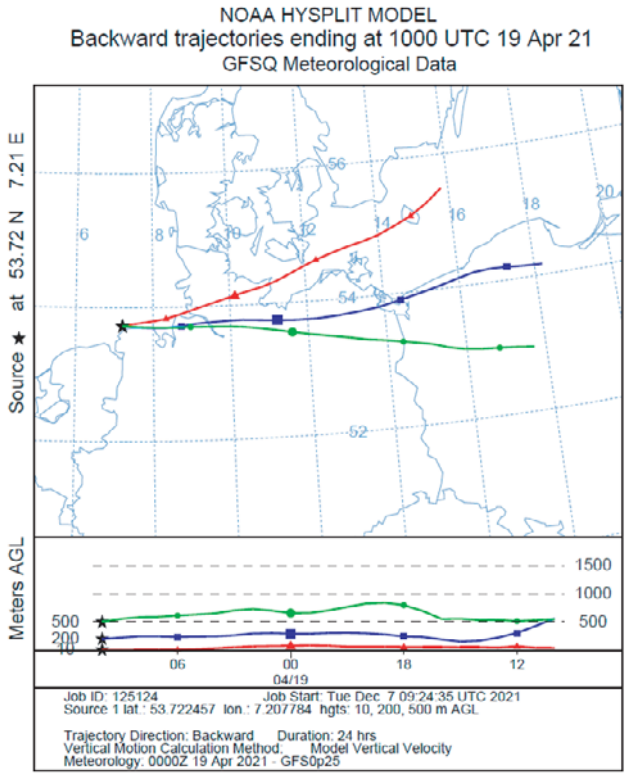

(a) 19th of April, 2021 (Norderney).

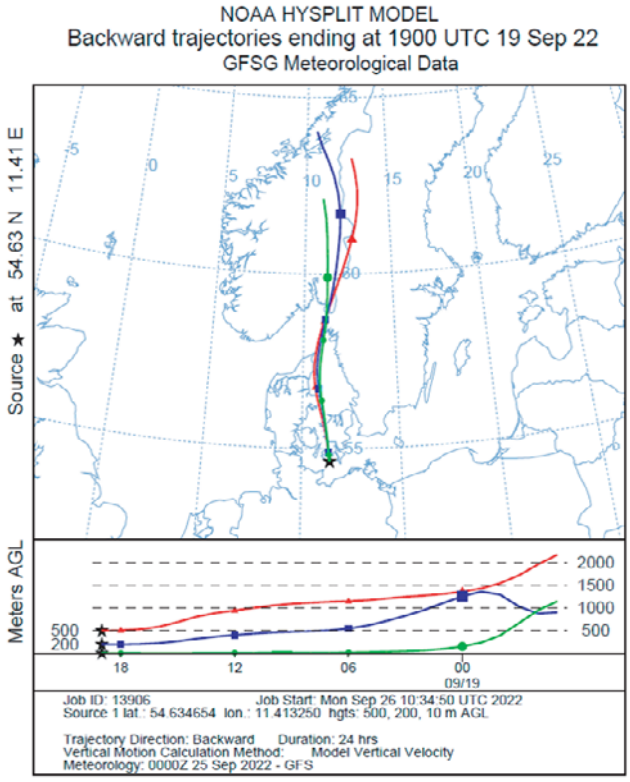

(b) 19th of September, 2022 (Rødby).

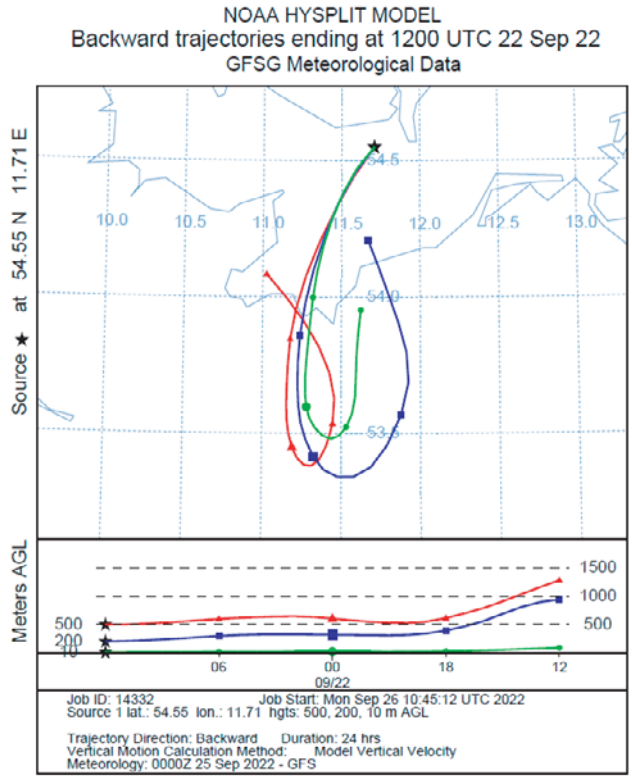

(c) 22nd of September, 2022 (Rødby).

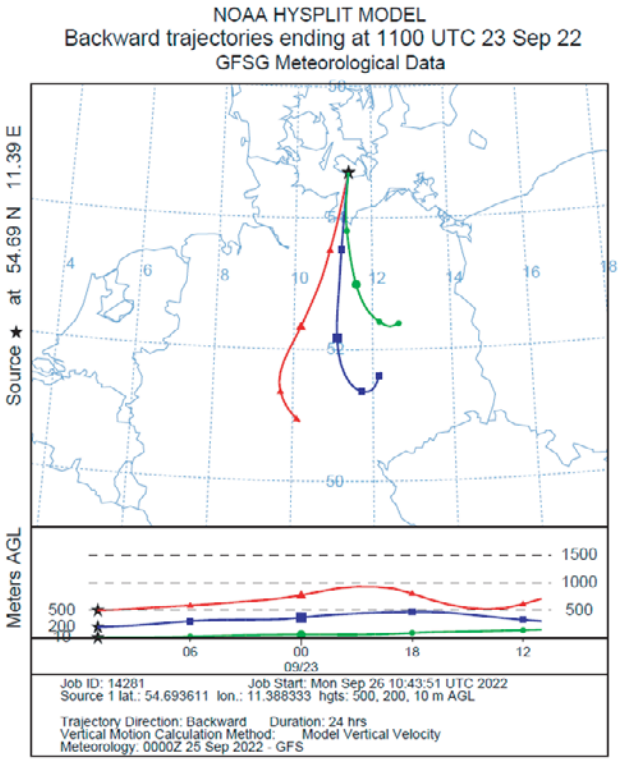

(d) 23rd of September, 2022 (Rødby).

Figure 3: Air mass 24-hour back trajectories for the cases of an urban aerosol source. The black star denotes the measurement location, which is also captioned below each figure, and the three lines indicate the origin of the air mass at three different altitudes, 10 m (light green), 200 m (dark blue) and 500 m (red).

dried air (fourth column in Table 1). The hygroscopicity parameter κ and growth factor GF were calculated according to the procedure described in Section 2.1, using RH measurements from the SHT31. PM_{water} is calculated with Eq. (2.5), and using PM_w and PM_d according to Table 1. Then, GF is calculated from Eq. (2.4) by using two values for particle density, $\rho_{as} = 1.77\,g \cdot cm^{-3}$ for ammonium sulphate and $\rho_{ss} = 2.1\,g \cdot cm^{-3}$ for sea salt. Afterwards, Eq. (2.2) is solved for κ by using the newly calculated growth factors. For each measurement period, 1-min mean values of all the related parameters were computed from the raw sensor outputs. A mean value of GF and κ was then calculated across the whole measurement period, and the uncertainty of the measurement was determined by calculating the corresponding standard deviation. Results were then compared to the growth factor curve in Figure 1 and the established κ values of each element. The governing difference between PM_d and PM_w dictates the outcome, because it reflects the hygroscopic behavior of the aerosol particle that is actually measured. Since the air mass type is known from HYSPLIT and shown in Figure 2–3, the method to identify it from PM data, as described in Section 2.1, is possible to be tested. To test the efficiency of the drying system when inter-comparing OPC-N3 and Fidas Fly 100, three OPCs were in operation for one of the measurement days, including the reference instrument and one OPC-N3 with a drying chamber, and one without. In this way, it could be investigated whether differences between ambient and dry measurements were solely because of the hygroscopic growth effect.

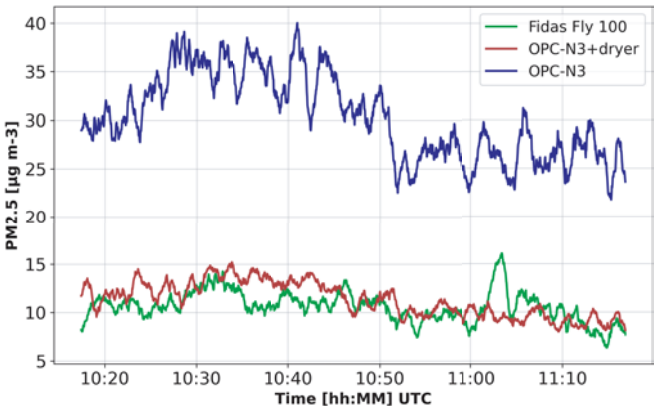

Figure 4: $PM_{2.5}$ time series for September 17th. The three OPCs included a reference instrument with a drying method (Fidas Fly 100 – green line), the OPC-N3 with a self-constructed diffusion drying chamber (dark red line) and an unmodified OPC-N3 that featured no drying (blue line).

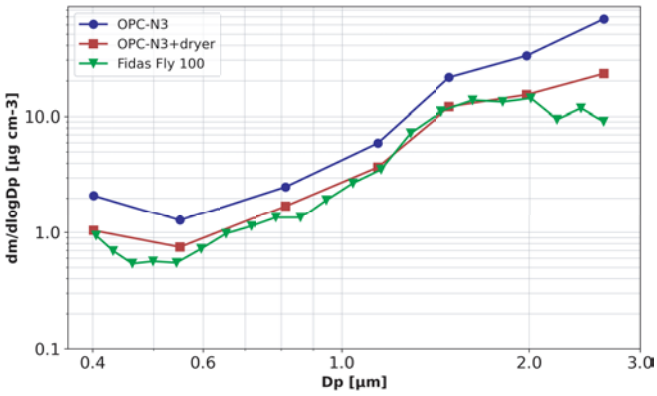

Figure 5: Particle mass size distributions for September 17th. The three OPCs included a reference instrument with a drying method (Fidas Fly 100 – green line), the OPC-N3 with a self-constructed diffusion drying chamber (dark red line) and an unmodified OPC-N3 that featured no drying (blue line).

3 Results

For the 17th of September 2022, the results of the $PM_{2.5}$ time series and mass distributions can be seen in Figure 4–5. A clear overestimation is evident for the case of the unmodified OPC-N3, which recorded almost three times higher $PM_{2.5}$ than the reference instrument (Figure 4). Similar is the case for the overestimation of the particle mass size distribution shown in Figure 5, demonstrating the effect of hygroscopic growth at humid conditions. For the case of the modified OPC-N3 with an added diffusion dryer, $PM_{2.5}$ is in better agreement with the reference instrument, with an overestimation of 21 % between 10:25–10:45 UTC. As observed at the mass distributions (Figure 5), there is a general consistency between OPC-N3 with a dryer and Fidas Fly 100, with an 16 % overestimation of the former up to sizes of 0.8 µm. Between the smaller sizes of 0.4–0.55 µm, the two instruments are in agreement at the points where they have exactly the same size boundary. The two instruments match well from 1 to 2 µm, and an overestimation of the OPC-N3 can be seen above 2 µm, with a maximum difference at the last size bin, which is however above 2.5 µm and therefore not accounted for when calculating $PM_{2.5}$. There is a distinct peak for a period of two minutes from the Fidas Fly 100 at 11:03 UTC, most likely from measuring particles smaller than what the OPC-N3 can detect. Figures 4–5 show comparable results between the Fidas Fly 100 and the OPC-N3 with its own drying method, and both were used for capturing PM_d at different measurement periods, as described in Table 1.

Calculated GF, κ and the expected κ values, according to Sections 2.1 & 2.3, are shown in Table 2. The computations for each day were based on time series equivalent to Figure 4, with PM_d being the measurements from the OPC-N2/N3+dryer or Fidas Fly 100, and PM_w were the measurements from the unmodified OPC-N2/N3. Columns 2–4 of Table 2 show the calculations for GF and κ. They are based on two different particle densities, sea salt (ρ_{ss}) and for ammonium sulphate (ρ_{as}), that reflect marine and urban background air respectively. A known κ for these two elements, from

Table 2: Calculated GF, κ using two particle densities (ρ_{ss}: density of sea salt, ρ_{as}: density of ammonium sulphate), and the average RH levels during the times of each measurement, for each data time period.

Date	**GF (ρ_{ss})**	**GF (ρ_{as})**	**$\kappa(\rho_{ss})$**	**$\kappa(\rho_{as})$**	$\overline{RH}$ [%]	κ_{ss} (Zieger et al., 2017)
17 Apr 21	1.83 ± 0.08	1.74 ± 0.08	1.0 ± 0.1	0.9 ± 0.2	83	1.1
16 Sep 22	1.61 ± 0.07	1.55 ± 0.06	1.1 ± 0.2	1.0 ± 0.2	74	1.1
17 Sep 22	1.74 ± 0.06	1.65 ± 0.05	1.1 ± 0.1	0.9 ± 0.1	80	1.1
21 Sep 22	1.4 ± 0.1	1.3 ± 0.1	1.1 ± 0.1	0.9 ± 0.1	63	1.1
						κ_{as} (Di Antonio et al., 2018)
19 Apr 21	1.38 ± 0.09	1.33 ± 0.08	0.8 ± 0.1	0.6 ± 0.1	68	0.61
19 Sep 22	1.5 ± 0.1	1.4 ± 0.1	0.8 ± 0.2	0.6 ± 0.2	76	0.61
22 Sep 22	1.17 ± 0.05	1.15 ± 0.06	0.7 ± 0.1	0.6 ± 0.1	47	0.61
23 Sep 22	1.31 ± 0.05	1.27 ± 0.05	0.8 ± 0.1	0.7 ± 0.1	61	0.61

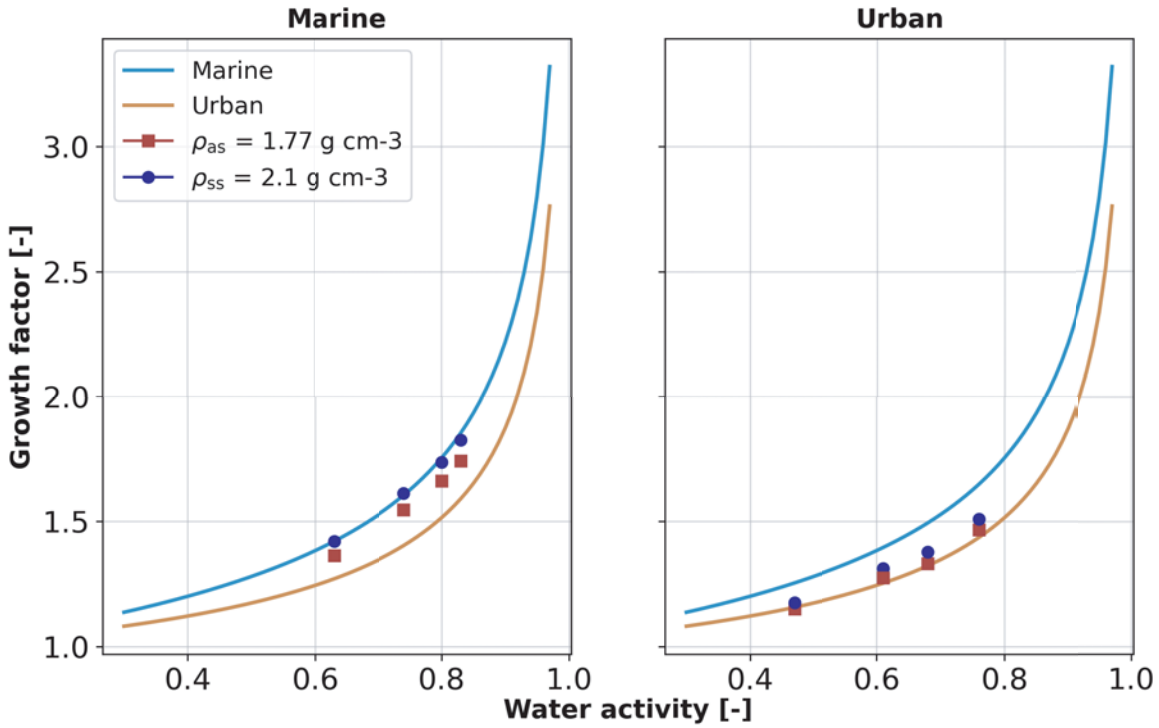

Figure 6: Growth factor curves as in Figure 1, but now limited to a range between a_w of 0.3 and 1. Each data point in the plot represents a different measurement day, and results are split in two categories, the cases when marine or urban air was present, according to Table 1. The average RH level is taken from the SHT31 measurements and shown in Column 6 of Table 2, as it is converted to water activity with Eq. (2.3). Two points per RH are shown, which are related to two growth factors, one using ρ_{as} and one from ρ_{ss}.

previous studies on the subject, is also shown and the two air mass origins are separated as in Table 1. It can be noted that when HYSPLIT displays air from the sea (Figure 2), calculated κ matches the expected value for sea salt perfectly, only when using with the appropriate particle density. The same holds for the case of air from land, as it can be seen in Figure 3. When unsuitable particle densities are inserted, the resulting κ is not close to either expected value.

This is a first hint of understanding the type of air mass that is sampled, starting only from PM data, and the point is further illustrated by applying the calculated GF values (columns 2 and 3 in Table 2) on the growth rate plots of Figure 1, which can be seen in Figure 6.

The same phenomenon is apparent from the data points in Figure 6, where each one is the outcome of each measurement time period from Tables 1 and 2. GF values fall on a different growth curve depending of the sampled background air, regardless of the choice of particle density.

A closer look for the study case in Rødby, where aerosol particle number size distributions are calculated from the raw data for both ambient and dry air samples during these days, is shown in Figure 7. The distributions vary slightly between the first and second part of the experiments, as different air masses were measured in each time. Distributions from the 16th and 17th show a bump between 1 and 2 µm, which is smoothed out dur-

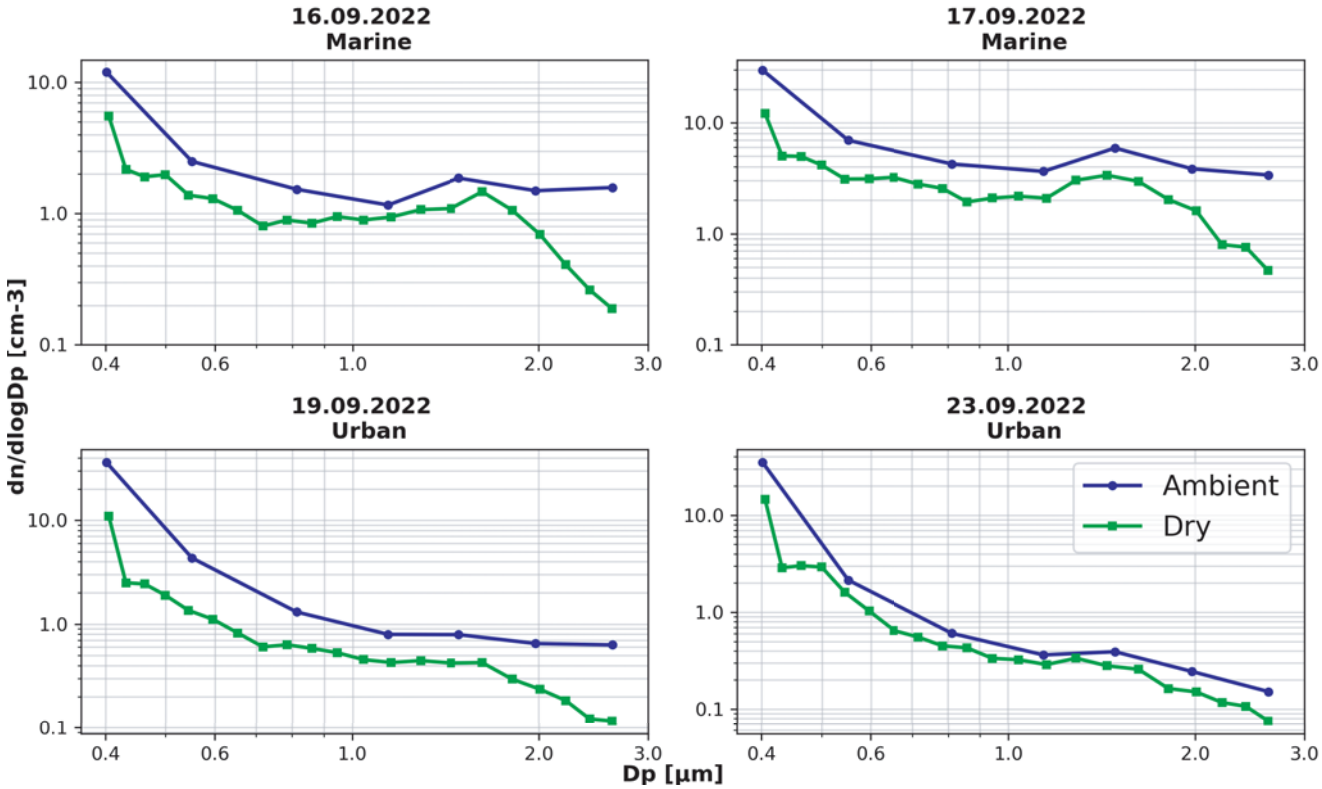

Figure 7: Particle number distributions for 4 measurement days, from the OPC-N3 (measuring ambient air) and the Fidas Fly 100 (measuring dry air). The distributions range from 0.4 to 3 µm particle geometric mean diameter size.

ing the cases with air from land, on the 19th and 23rd of September in Figure 7. The hygroscopic growth effect is evident everywhere, as number concentrations from the Fidas Fly 100 are lower across all bins in this size range.

Figure 2 shows simulations of the air mass back trajectories 24 hours prior to the measurements at the area of Rødby. It can be seen that for the 16th and 17th of September, the origins of the air mass are from the Northwest in the North Sea at all three presented altitudes, hardly passing any land until their arrival at Rødby. At the same time, for the 19th of September, the air mass came from a clearer northerly direction passing inland Norway and Sweden, and on the 23rd of September the source of the air mass can be tracked to the South, inside Germany. These two different air mass origins suggest a similar conclusion like Table 2 and Figure 6, which show an analogous resulting hygroscopicity parameter and growth factor that can be distinguished in each situation.

4 Discussion

The method proposed in this paper aims for estimating hygroscopic properties of aerosol particles, specifically the growth factor GF and hygroscopicity parameter κ, from $PM_{2.5}$ data and by taking advantage of the fundamental definition of GF, as it is stated with Eq. (2.1). As it can be identified in Table 2, the calculated κ for sea salt through Eq. (2.2) & (2.4) resulted in $\kappa_{ss} = 1.1$ when using the appropriate particle density, which is in agreement with a recent study that suggested the same value for numerical models (Zieger et al., 2017). For ammonium sulphate, $\kappa_{as} = 0.6$ is also aligned with previous studies on the element or a mixed urban aerosol with it as a dominant component (Svenningsson et al., 2006; Di Antonio et al., 2018), where values ranged between 0.61 and 0.62. It is important to remark that the hygroscopic growth curves for Figure 1 were produced by using the literature numbers for κ, yet the procedure to estimate them with our data begins from the difference of dry and wet PM measurements. This works as an affirmation to the already established values.

Prior to the calculation of κ, GF was found from Eq. (2.4) through $PM_{2.5}$ readings from the two sensors. A range of different RH levels was ongoing during the measurements, from 47 to 83 %, which allowed for a GF computation for different points on the curves of Figure 1. With the use of the applicable particle density, points for each measurement day agree with the expected growth factor of the given particle, basically showing that these kind of aerosol particles were being sampled that day. If the inappropriate particle density is used, the result is still closer to the correct growth curve related to the sampled air mass. As different densities are being tested, the results in GF and κ from Table 2

indicate that when using the expected particle density, both κ and GF match their anticipated values but if a non-appropriate particle density is used, neither κ or GF have any relevance with any of the two components. For example, for the case of the 19th of September, GF (ρ_{as}) = 1.4 matches the brown curve in Figure 6 at the average RH amount of the time of measurements, but the value GF (ρ_{ss}) = 1.5 doesn't match the blue curve, and the same can be seen for κ: 0.6 is close to the expected value if ammonium sulphate is the measured aerosol particle (when using ρ_{as}), while 0.8 is neither correct for sea salt or ammonium sulphate. This demonstrates that GF will be calculated correctly, when the appropriate density is inserted in Eq. (2.4), but if a different value (i.e. considering the growth of a certain particle type, but using a density of another), the resulting GF will still be in the vicinity of the correct curve and κ will match neither. Outcomes when using an appropriate value for density match their GF curves, and the following calculation of κ agrees with previously known values.

The results of this study are supported by the 24-hour back trajectories for each day, which show the same situation when it comes to the origin of the air mass. When an air mass from the sea is sampled (Figure 2a–2d), the proper κ and GF values are in turn calculated and agree with theory, but when the air mass originates from land (Figure 3a–3d), the hygroscopic properties are closer to what one would expect from an air sample that contains ammonium sulphate and not sea salt. A difference between these two is also clear from the particle number size distributions in Figure 7, which shows a slightly different structure between the first and last two days of the measurement period. The small "hill" identified in the first two days at sizes between 1 and 2 µm, represents a size distribution from water in the North and Baltic Sea, and it is reminiscent to other studies that have computed such size distributions in the area, predominantly occupied by sea salt from breaking waves, e.g. in Clarke et al. (2003). Specifically for the case in Figure 2a, while air masses higher above do pass from land, at 10 m altitude (red colored line) the trajectory shows a path only above water, which justifies how the ground measurements captured hygroscopic properties that are more similar to a marine based aerosol source. For that case, since higher altitude layers contain continental air mass which is less hygroscopic, the resulting $\kappa = 1 \pm 0.1$ is lower but still within the margin of the expected value of pure sea salt, which gives the verdict of an air sample mainly comprised of sea salt, yet mixed with non-marine air as well. On the last two days of the experiments in Rødby, the air mass originates from Scandinavia and Germany, more related to a mixed / polluted environment with its applicable size distribution. An extensive study on the chemical composition of $PM_{2.5}$ in north Taiwan for a year in 2016–2017 by Cheung et al. (2020), found κ values up to 0.56 related to an urban polluted environment with various pollutants. This work's result of $\kappa = 0.6$ matches better the hygroscopicity parameter of ammonium sulphate only ($\kappa = 0.61$), and it can be concluded that the air masses originating from land contained such aerosol particles for sizes up to 2.5 µm.

The method proposed aims for a direct way to estimate hygroscopic properties of aerosol particles, specifically the growth factor GF and hygroscopicity parameter κ, from direct sensor $PM_{2.5}$ data and by taking advantage of the fundamental definition of GF, as it is stated with Eq. (2.1). The assumption of particle spherical shape is maintained in this process, but it is a generally accepted notion that is taken into account when it comes to most aerosol particle analysis or PM calculation by instruments such as an OPC. A discrepancy in the measurements could lie in the fact that each sensor usually assumes its own complex refractive index for particle characterization, for this the OPC-N3 considers a value of $n = 1.5 + 0i$ (Alphasense, 2019) and for the Fidas Fly 100 in its standard mode it is $n = 1.59 + 0i$. For the specific experiments, PM_1 was avoided because of the difference in the sensors' lower bin size: 0.18 µm for the Fidas Fly 100 and 0.35 µm for the OPC-N3. This remains as a potential indirect comparison error. Hegg et al. (2006) noted a slight difference in GF values between aerosol particles in the sub-micrometer and micrometer range at certain RH conditions, while $PM_{2.5}$ of course considers all aerosol particles up to an aerodynamic diameter of 2.5 µm. Nevertheless, results from the current study showed that the calculation steps described in Section 2.1 can provide an accurate estimation for κ and GF, as it can be concluded when looking at the air mass back trajectories in Figure 2, and combining them with the points in Figure 6 and contents of Table 2. When comparing an OPC-N3 with a drying channel and the Fidas Fly 100, results were in agreement with each other as seen in Figure 4–5. This demonstrates how the overestimation of the unmodified OPC-N3 compared to either the OPC-N3 + dryer or reference instrument, is widely due to the effect of RH on the apparent size of the sampled aerosol particles.

5 Conclusions

A concise method is presented for the calculation of GF and κ using $PM_{2.5}$ from two aerosol particle optical sensors. One of them features a drying system and one does not, and the difference between ambient and dried PM concentrations are used through Eq. (2.1) to calculate GF and κ. Eq. (2.2), which relates GF and different RH levels through κ only (Petters and Kreidenweis, 2007; Di Antonio et al., 2018), is used for connecting all parameters together and plotting theoretical growth curves for specific elements (Figure 1). Using measurements on an island in the North Sea (Norderney, Germany) and at the coast of South Denmark and near the Baltic Sea, these aerosol particle hygroscopic properties were calculated by using an OPC-N2/N3 (with and without a drying chamber) and a Fidas Fly 100 (with a drying chamber). Results showed that $\kappa = 0.6 \pm 0.1$ when

the measured air mass had an urban origin, indicating aerosol particles predominantly with ammonium sulphate, a typical component of polluted air. When measuring air from the sea, the hygroscopicity parameter was found to be $\kappa = 1.1 \pm 0.1$, which agrees with the value expected for abundant sea salt in the sample.

Accordingly, growth factors matched their appropriate curves with a distinction between the two cases (marine and urban aerosol) for various RH levels, which were all above the efflorescence points of both sea salt and ammonium sulphate, hence the presence of hygroscopic growth. The origin of the air masses was tracked by simulating back trajectories from the NOAA HYSPLIT model 24 hours before the measurements, which show the times when the air mass was of urban or marine source and agree with the hygroscopic growth differences expected for sea salt and ammonium sulphate. Particle number size distributions also show a notable difference, with the case of marine aerosol from the Baltic and North Sea, a small peak in number concentrations is seen at sizes of 1–2 µm.

As strictly defining the chemical composition of aerosol particles would require a cascade impactor, this method provides insight on aerosols through their hygroscopic properties at least to the level of air mass origin. This also extends the size range where such properties are studied, as mostly the hygroscopic growth effect is present in ranges often much lower that what typical OPCs cover, aerosol particle sizes with an aerodynamic diameter at the order of magnitude from few to few hundreds of nanometers. By combining ambient and dry PM data collection, a sensor otherwise blind to particle composition and air mass origin, can be used to provide such information by taking advantage of the hygroscopic growth effect. As low-cost OPCs without the inclusion of a drying chamber have been under development during the last few years for air quality research, our method could prove useful when expensive instrumentation, specifically for hygroscopic growth analysis, is unavailable.

Acknowledgements

The authors would like to thank the off-shore Wind Park company RWE for their hospitality on the maintenance vessels of the off-shore wind park Rodsand II during September 2022, where parts of the acquired measurements were obtained. We would also like to thank the Train2Wind Innovation Network for the collaboration and partial financial support of this project.

Declaration of competing interest

The authors declare that they have no conflict of interest.

Data availability statement

Data, post-processing scripts, and data acquisition scripts can be provided from the corresponding author upon reasonable request.

Funding

This work is partly funded by the European Union Horizon 2020 research and innovation program under grant agreement no. 861291 as part of the Train2Wind Marie Sklodowska-Curie Innovation Training Network (https://www.train2wind.eu/)

Appendix

A Diffusion dryer

The diffusion dryer attached on the low-cost OPCs of this study was a self-constructed dryer, and subject of another publication (Savvakis et al., 2024). A short description and details of dimensions are given here.

A.1 Specifications

The drying channel is based on the concept of diffusion drying, and consists of two co-axial tubes. The inner tube is perforated while the outer tube is solid, and in between a dessicant is placed, in this case blue silica beads. The inner tube has the same diameter as the inlet of the OPC-N2 or OPC-N3, and it is attached to it in a way that the connection is airtight. All the components have been designed with Computer Aided Design (CAD) programming and 3-D printed.

Characteristics of the dryer can be found the following table, taken from Savvakis et al. (2024):

	Inner tube	**Outer tube**
Inner diameter [mm]	6.2	20
Outer diameter [mm]	6.5	23
Material	Liquid Resin	Poly Lactic Acid (PLA)
Length [mm]	120	99

List of Abbreviations

GF	Growth factor
H-TDMA	Hygroscopic Tandem Differential Mobility Analyzer
HYSPLIT	Hybrid Single-Particle- Langrangian Integrated Trajectory
IADS	Intelligent Aerosol Drying System
OAS	Optical aerosol spectrometer
OPC	Optical particle counter
PM	Particulate matter
PNC	Particle number concentration
RH	Relative humidity

References

Alphasense, L., 2015: User Manual: OPC-N2 Optical Particle Counter. https://www.manualslib.com/manual/1540841/Alphasense-Opc-N2.html (Accessed on December 12th, 2022).

Alphasense, L., 2019: User Manual: OPC-N3 Optical Particle Counter.. https://www.alphasense.com/wp-content/uploads/2019/03/OPC‑N3.pdf (Accessed on October 14th, 2022).

Biskos, G., A. Malinowski, L. Russell, P. Buseck, S. Martin, 2006: Nanosize effect on the deliquescence and the efflorescence of sodium chloride particles. – Aerosol Sci. Technol. **2**, 97–106, DOI: 10.1080/02786820500484396.

Bohren, C.F., D.R. Huffman, 2008: Absorption and scattering of light by small particles – John Wiley & Sons.

Cheung, H.C., C.C.K. Chou, C.S.L. Lee, W.C. Kuo, S.C. Chang, 2020: Hygroscopic properties and cloud condensation nuclei activity of atmospheric aerosols under the influences of Asian continental outflow and new particle formation at a coastal site in Eastern Asia. – Atmos. Chem. Phys. **10**, 5911–5922, DOI: 10.5194/acp-20-5911-2020.

Clarke, A., V. Kapustin, S. Howell, K. Moore, B. Lienert, S. Masonis, T. Anderson, D. Covert, 2003: Sea-salt size distributions from breaking waves: Implications for marine aerosol production and optical extinction measurements during SEAS. – J. Atmos. Ocean. Technol. **10**, 1362–1374, DOI: 10.1175/1520-0426(2003)020<1362:SSDFBW>2.0.CO;2.

Crilley, L.R., A. Singh, L.J. Kramer, M.D. Shaw, M.S. Alam, J.S. Apte, W.J. Bloss, L. Hildebrandt Ruiz, P. Fu, W. Fu, others, 2020: Effect of aerosol composition on the performance of low-cost optical particle counter correction factors. – Atmos. Measur. Techniq. **3**, 1181–1193.

Davies, J.F., C.L. Price, J. Choczynski, R.K. Kohli, 2021: Hygroscopic growth of simulated lung fluid aerosol particles under ambient environmental conditions. – Chemical Commun. **26**, 3243–3246, DOI: 10.1039/D1CC00066G.

Di Antonio, A., O.A. Popoola, B. Ouyang, J. Saffell, R.L. Jones, 2018: Developing a relative humidity correction for low-cost sensors measuring ambient particulate matter. – Sensors **9**, 2790, DOI: 10.3390/s18092790.

Drake, R., J. Gordon, 1985: Mie scattering. – Amer. J. Phys. **10**, 955–962, DOI: 10.1119/1.14011.

Feingold, G., B. Morley, 2003: Aerosol hygroscopic properties as measured by lidar and comparison with in situ measurements. – J. Geophys. Res. Atmos. **D11**, DOI: 10.1029/2002JD002842.

Fitzgerald, J.W., 1975: Approximation formulas for the equilibrium size of an aerosol particle as a function of its dry size and composition and the ambient relative humidity. – J. Appl. Meteor. Climatol. **6**, 1044–1049, DOI: 10.1175/1520-0450(1975)014<1044:AFFTES>2.0.CO;2.

Griffiths, P., J.S. Borlace, P. Gallimore, M. Kalberer, M. Herzog, F. Pope, 2012: Hygroscopic growth and cloud activation of pollen: A laboratory and modelling study. – Atmos. Sci. Lett. **4**, 289–295, DOI: 10.1002/asl.397.

Gupta, D., H.J. Eom, H.R. Cho, C.U. Ro, 2015: Hygroscopic behavior of NaCl–MgCl 2 mixture particles as nascent seaspray aerosol surrogates and observation of efflorescence during humidification. – Atmos. Chem. Phys. **19**, 11273–11290, DOI: 10.5194/acp-15-11273-2015.

Gysel, M., J. Crosier, D. Topping, J. Whitehead, K. Bower, M. Cubison, P. Williams, M. Flynn, G. McFiggans, H. Coe, 2007: Closure study between chemical composition and hygroscopic growth of aerosol particles during TORCH2. – Atmos. Chem. Phys. **24**, 6131–6144, DOI: 10.5194/acp-7-6131-2007.

Hagan, D.H., J.H. Kroll, 2020: Assessing the accuracy of low-cost optical particle sensors using a physics-based approach. – Atmos. Measur. Techniq. **11**, 6343–6355, DOI: 10.5194/amt-13-6343-2020.

Hämeri, K., M. Väkevä, H.C. Hansson, A. Laaksonen, 2000: Hygroscopic growth of ultrafine ammonium sulphate aerosol measured using an ultrafine tandem differential mobility analyzer. – J. Geophys. Res. Atmos.**D17**, 22231–22242.

Hämeri, K., A. Laaksonen, M. Väkevä, T. Suni, 2001: Hygroscopic growth of ultrafine sodium chloride particles. – J. Geophys. Res. Atmos. **D18**, 20749–20757, DOI: 10.1029/2000JD900220.

Hegg, D., D.S. Covert, K. Crahan, H. Jonsson, Y. Liu, 2006: Measurements of aerosol size-resolved hygroscopicity at sub and supermicron sizes. – Geophys.Res. Lett. **21**, DOI: 10.1029/2006GL026747.

Hitzenberger, R., A. Berner, U. Dusek, R. Alabashi, 1997: Humidity-dependent growth of size-segregated aerosol samples. – Aerosol Sci. Technol. **21**, 116–130, DOI: 10.1080/02786829708965461.

Kaaden, N., A. Massling, A. Schladitz, T. Müller, K. Kandler, L. Schütz, B. Weinzierl, A. Petzold, M. Tesche, S. Leinert, others, 2009: State of mixing, shape factor, number size distribution, and hygroscopic growth of the Saharan anthropogenic and mineral dust aerosol at Tinfou, Morocco. – Tellus B: Chem. Phys. Meteor. **1**, 51–63, DOI: 10.1111/j.1600-0889.2008.00388.x.

Kitamori, Y., M. Mochida, K. Kawamura, 2009: Assessment of the aerosol water content in urban atmospheric particles by the hygroscopic growth measurements in Sapporo, Japan. – Atmos. Env. **21**, 3416–3423, DOI: 10.1016/j.atmosenv.2009.03.037.

Laskina, O., H.S. Morris, J.R. Grandquist, Z. Qin, E.A. Stone, A.V. Tivanski, V.H. Grassian, 2015: Size matters in the water uptake and hygroscopic growth of atmospherically relevant multicomponent aerosol particles. – J. Phys. Chem. A **19**, 4489–4497.

Liu, B., D. Pui, K. Whitby, D.B. Kittelson, Y. Kousaka, R. McKenzie, 1978: The aerosol mobility chromatograph: a new detector for sulfuric acid aerosols. – In: Sulfur in the atmosphere, Elsevier, 99–104.

Malings, C., R. Tanzer, A. Hauryliuk, P.K. Saha, A.L. Robinson, A.A. Presto, R. Subramanian, 2020: Fine particle mass monitoring with low-cost sensors: Corrections and long-term performance evaluation. – Aerosol Sci. Technol. **2**, 160–174, DOI: 10.1080/02786826.2019.1623863.

Ming, Y., L.M. Russell, 2001: Predicted hygroscopic growth of sea salt aerosol. – J. Geophys. Res. Atmos. **D22**, 28259–28274, DOI: 10.1029/2001JD000454.

Molnár, A., K. Imre, Z. Ferenczi, G. Kiss, A. Gelencsér, 2020: Aerosol hygroscopicity: Hygroscopic growth proxy based on visibility for low-cost PM monitoring. – Atmos. Res. **236**, 104815, DOI: 10.1016/j.atmosres.2019.104815.

Petters, M., S. Kreidenweis, 2007: A single parameter representation of hygroscopic growth and cloud condensation nucleus activity. – Atmos. Chem. Phys. **8**, 1961–1971, DOI: 10.5194/acp-7-1961-2007.

Savvakis, V., M. Schön, M. Bramati, B. Jens, A. Platis, 2024: Small-scale diffusion dryer on an optical particle counter for high humidity aerosol measurements with an uncrewed aircraft system. – accepted by J. Atmos. Ocean. Technol.

Sensirion, S., 2016: Sensor datasheet: SHT31.. https://sensirion.com/media/documents/213E6A3B/63A5A569/Datasheet_SHT3x_DIS.pdf (Accessed on November 22nd, 2023).

Snider, J.R., M.D. Petters, 2008: Optical particle counter measurement of marine aerosol hygroscopic growth. – Atmos. Chem. Phys. **7**, 1949–1962, DOI: 10.5194/acp-8-1949-2008.

Sorjamaa, R., A. Laaksonen, 2007: The effect of H_20 adsorption on cloud drop activation of insoluble particles: a theoretical framework. – Atmos. Chem. Phys. **24**, 6175–6180, DOI: 10.5194/acp-7-6175-2007.

Stein, A.F., R.R. Draxler, G.D. Rolph, B.J.B. Stunder, M.D. Cohen, F. Ngan, 2015: NOAA's HYSPLIT

atmospheric transport and dispersion modeling system. – Bull. Amer. Meteor. Soc.**12**, 2059–2077, DOI: 10.1175/BAMS-D-14-00110.1.

Svenningsson, B., J. Rissler, E. Swietlicki, M. Mircea, M. Bilde, M. Facchini, S. Decesari, S. Fuzzi, J. Zhou, J. Mønster, others, 2006: Hygroscopic growth and critical supersaturations for mixed aerosol particles of inorganic and organic compounds of atmospheric relevance. – Atmos. Chem. Phys. **7**, 1937–1952, DOI: 10.5194/acp-6-1937-2006.

Swietlicki, E., H.C. Hansson, K. Hämeri, B. Svenningsson, A. Massling, G. McFiggans, P. McMurry, T. Petäjä, P. Tunved, M. Gysel, others, 2008: Hygroscopic properties of submicrometer atmospheric aerosol particles measured with H-TDMA instruments in various environments – a review. – Tellus B: Chem. Phys. Meteor. **3**, 432–469, DOI: 10.1111/j.1600-0889.2008.00350.x.

Tang, I.N., A. Tridico, K. Fung, 1997: Thermodynamic and optical properties of sea salt aerosols. – J. Geophys. Res. Atmos. **D19**, 23269–23275.

Tang, M., C.K. Chan, Y.J. Li, H. Su, Q. Ma, Z. Wu, G. Zhang, Z. Wang, M. Ge, M. Hu, others, 2019: A review of experimental techniques for aerosol hygroscopicity studies. – Atmos. Chem. Phys. **19**, 12631–12686, DOI: 10.5194/acp-19-12631-2019.

Turšič, J., B. Podkrajšek, I. Grgić, P. Ctyroky, A. Berner, U. Dusek, R. Hitzenberger, 2006: Chemical composition and hygroscopic properties of size-segregated aerosol particles collected at the Adriatic coast of Slovenia. – Chemosphere **7**, 1193–1202, DOI: 10.1016/j.chemosphere.2005.08.040.

Weingartner, E., H. Burtscher, U. Baltensperger, 1997: Hygroscopic properties of carbon and diesel soot particles. – Atmos. Env. **15**, 2311–2327, DOI: 10.1016/S1352-2310(97)00023-X.

Won, W.S., R. Oh, W. Lee, S. Ku, P.C. Su, Y.J. Yoon, 2021: Hygroscopic properties of particulate matter and effects of their interactions with weather on visibility. – Sci. Rep. **1**, 1–12, DOI: 10.1038/s41598-021-95834-6.

Zhao, P., J. Ding, X. Du, J. Su, 2019: High time-resolution measurement of light scattering hygroscopic growth factor in Beijing: A novel method for high relative humidity conditions. – Atmos. Env. **215**, 116912, DOI: 10.1016/j.atmosenv.2019.116912.

Zieger, P., O. Väisänen, J.C. Corbin, D.G. Partridge, S. Bastelberger, M. Mousavi-Fard, B. Rosati, M. Gysel, U.K. Krieger, C. Leck, others, 2017: Revising the hygroscopicity of inorganic sea salt particles. – Nature Comm. **1**, 1–10, DOI: 10.1038/ncomms15883.